Bistability in a nonequilibrium quantum system with electron-phonon interactions

Eli Y. Wilner, Haobin Wang, Guy Cohen, Michael Thoss, and Eran Rabani

Phys. Rev. B **88**, 045137 — Published 31 July 2013

DOI: 10.1103/PhysRevB.88.045137

Bistability in a nonequilibrium quantum system with electron-phonon interactions

Eli Y. Wilner,[1] Haobin Wang,[2] Guy Cohen,[3] Michael Thoss,[4] and Eran Rabani[5]

[1]*School of Physics and Astronomy, The Sackler Faculty of Exact Sciences, Tel Aviv University,Tel Aviv 69978,Israel*
[2]*Department of Chemistry and Biochemistry, New Mexico State University, Las Cruces, NM 88003, USA*
[3]*Department of Physics and Chemistry, Columbia University, New York, New York 10027, USA*
[4]*Institute for Theoretical Physics and Interdisciplinary Center for Molecular Materials, Friedrich-Alexander-Universität Erlangen-Nürnberg, Staudtstr. 7/B2, D-991058 Erlangen, Germany*
[5]*School of Chemistry, The Sackler Faculty of Exact Sciences, Tel Aviv University,Tel Aviv 69978,Israel*

The existence of more than one steady-state in a many-body quantum system driven out-of-equilibrium has been a matter of debate, both in the context of simple impurity models and in the case of inelastic tunneling channels. In this paper, we combine a reduced density matrix formalism with the multilayer multiconfiguration time-dependent Hartree method to address this problem. This allows us to obtain a converged numerical solution of the nonequilibrium dynamics. Considering a generic model for quantum transport through a quantum dot with electron-phonon interaction, we prove that a unique steady-state exists regardless of the initial electronic preparation of the quantum dot, consistent with the converged numerical results. However, a bistability can be observed for different initial phonon preparations. The effects of the phonon frequency and strength of the electron-phonon couplings on the nonequilibrium dynamics and on the emergence of bistability is discussed.

I. INTRODUCTION

The existence of a unique steady-state in strongly correlated quantum systems out-of-equilibrium is a subject of great interest and controversy. For the case of the Anderson impurity model, it has been argued using the Bethe ansatz that a single steady-state solution exists[1]. However, recent calculations of the nonequilibrium current based on time-dependent density functional theory seem to indicate that at long times the system reaches a dynamical state characterized by correlation-induced current oscillations[2]. Similarly, questions regarding hysteresis, bistability and the dependence of the steady-state current on the initial occupation have been raised in the context of inelastic transport through nanoscale quantum dots[3–11].

Addressing the issue of a unique steady-state is a challenging task for theory, as systems exhibiting bistability involve strong electron-electron or electron-phonon correlations. Under these conditions, an exact solution is unavailable, and one has to resort to approximate methods or to numerical techniques. The former are based on either a mean-field approximation or perturbative schemes, where the inclusion of higher order corrections is not always clear or systematic, and thus may lead to questionable results. Numerical brute-force approaches, such as time-dependent numerical renormalization-group techniques[12–15], iterative[16–18] or stochastic[19–22] diagrammatic methods, and wave function based approaches[23], have been very fruitful, but are limited in the range of parameters and timescales that can be studied.

In this paper, we address the problem of bistability and a unique steady-state in a system with electron-phonon interaction under nonequilibrium conditions caused by a finite bias. We develop an approach based on a reduced density matrix (RDM) formalism, which requires as input a short-lived memory kernel[24]. The formalism is combined with the multilayer multiconfiguration time-dependent Hartree method (ML-MCTDH)[25] to numerically converge the memory kernel at short times until it decays, and infer from it the dynamics of the system at longer times and the approach to steady-state. Our approach offers a numerically exact description of the dynamics of a quantum system driven out-of-equilibrium on timescales not previously accessible. The RDM formalism provides us with means to prove analytically that if a steady-state exists then it must be unique, regardless of the initial electronic preparation. However, a bistability can develop for different initial phonon states. The relaxation to steady-state and the appearance of the bistability depends on the phonon frequency and the strength of the electron-phonon couplings.

II. MODEL

We consider a generic model for charge transport through a quantum dot with electron-phonon interaction.[26] The model is described by the Hamiltonian

$$H = H_S + H_B + V_{SB}, \tag{1}$$

where

$$H_S = \varepsilon_d d^\dagger d \tag{2}$$

is the system (quantum dot) Hamiltonian with creation/annihilation fermionic operators $d^\dagger/d$ and energy ε_d, $H_B = H_l + H_{\rm ph}$ where

$$H_l = \sum_{k\in L,R} \varepsilon_k a_k^\dagger a_k \tag{3}$$

represents the noninteracting leads Hamiltonian with fermionic creation/annihilation operators $a_k^\dagger/a_k$, and

$$H_{\rm ph}=\sum_\alpha \omega_\alpha\left(b_\alpha^\dagger b_\alpha+\frac{1}{2}\right) \tag{4}$$

represents the phonon bath with creation/annihilation bosonic operators $b_\alpha^\dagger/b_\alpha$ for phonon mode α with energy ω_α. The coupling between the system and the baths is given by $V_{SB}=V_l+V_{\rm ph}$ where

$$V_l=\sum_{k\in L,R}\left(t_k d a_k^\dagger+t_k^* a_k d^\dagger\right) \tag{5}$$

is the coupling between the system and the leads with couplings strength t_k, and

$$V_{\rm ph}=d^\dagger d\sum_\alpha M_\alpha\left(b_\alpha^\dagger+b_\alpha\right) \tag{6}$$

is the couplings between the system and the phonon bath, where M_α is the electron-phonon couplings to mode α.

The coupling strengths were parameterized by various spectral functions. The dot-leads coupling terms were determined from the spectral density

$$\Gamma_{L,R}(\varepsilon)=2\pi\sum_{k\in L,R}|t_k|^2\delta(\varepsilon-\varepsilon_k)=\frac{a^2}{b^2}\sqrt{4b^2-(\varepsilon-\mu_{L,R})^2}, \tag{7}$$

where a tight-binding model was employed, with $a=0.2$eV and $b=1$eV. $\mu_{L,R}$ is the chemical potential of the left (L) or right (R) lead, respectively. Similarly, the electron-phonon couplings were determined from a phonon spectral function

$$J(\omega)=\pi\sum_\alpha M_\alpha^2\delta(\omega-\omega_\alpha)=\frac{\pi}{2}\eta\omega e^{-\frac{\omega}{\omega_c}} \tag{8}$$

taken to be of Ohmic form. The dimensionless Kondo parameter, $\eta=\frac{2\lambda}{\omega_c}$, determines the overall strength of the electron-phonon couplings where $\lambda=\sum\frac{M_\alpha^2}{\omega_\alpha}=\frac{1}{\pi}\int\frac{d\omega}{\omega}J(\omega)$ is the reorganization energy (or polaron shift) and ω_c is the characteristic phonon bath frequency.

III. REDUCED DYNAMICS

Following the derivation outlined in Ref. 24 for the Anderson impurity model, the equation of motion for the RDM of the quantum dot, $\sigma(t)=Tr_B\{\rho(t)\}$, is given by

$$i\hbar\frac{\partial}{\partial t}\sigma\left(t\right)=\mathcal{L}_S\sigma\left(t\right)+\vartheta\left(t\right)-\frac{i}{\hbar}\int_0^t d\tau\kappa\left(\tau\right)\sigma\left(t-\tau\right) \tag{9}$$

where $\mathcal{L}_S=[H_S,\cdots]$ is the system's Liouvillian, $Tr_B\{\cdots\}$ is a trace over the baths degrees of freedom (leads and phonon baths) and $\rho(t)$ is the full density matrix. In the above,

$$\vartheta\left(t\right)=Tr_B\left\{\mathcal{L}_V e^{-\frac{i}{\hbar}Q\mathcal{L}t}Q\rho\left(0\right)\right\} \tag{10}$$

depends on the choice of initial conditions and vanishes for an uncorrelated initial state (which is the case discussed below), *i.e.* when $\rho(0)=\sigma(0)\otimes\rho_B(0)$, where $\sigma(0)$ and $\rho_B(0)$ are the system and baths initial density matrices, respectively, and $\mathcal{L}_v=[V_{SB},\cdots]$. The memory kernel, which describes the non-Markovian dependency of the time propagation of the system, is given by

$$\kappa\left(t\right)=Tr_B\left\{\mathcal{L}_V e^{-\frac{i}{\hbar}Q\mathcal{L}t}Q\mathcal{L}\rho_B\right\} \tag{11}$$

where $Q=1-P$, $P=\rho_B(0)Tr_B\{\cdots\}$ and $\mathcal{L}=[H,\cdots]$.

To obtain $\sigma(t)$, one requires as input the super-matrix of the memory kernel, which can be expressed in terms of a Volterra equation of the second type, removing the complexity of the projected dynamics of Eq. (11):[27]

$$\kappa\left(t\right)=i\hbar\dot{\Phi}\left(t\right)-\Phi\left(t\right)\mathcal{L}_S+\frac{i}{\hbar}\int_0^t d\tau\Phi\left(t-\tau\right)\kappa\left(\tau\right) \tag{12}$$

with

$$\Phi\left(t\right)=Tr_B\left\{\mathcal{L}_V e^{-\frac{i}{\hbar}\mathcal{L}t}\rho_B\right\}. \tag{13}$$

Evaluating the super-matrix $\Phi(t)$ requires a calculation analogous to that carried out in Ref. 24 for the Anderson impurity model.

For the present model, it can be shown that the populations and coherences of $\sigma(t)$ are decoupled, and if one is interested in the behavior of the populations alone, only the diagonal elements of $\Phi_{ii,mm}(t)$ are required. These can be expressed in terms of the sum of the left and right currents $\Phi_{ii,mm}(t)=-i\frac{\hbar}{e}(I_m^L(t)+I_m^R(t))$, where

$$I_m^{L,R}(t)=-\frac{2e}{\hbar}\Im\left\{\sum_{k\in L,R}t_k\langle m|d(t)a_k^\dagger(t)|m\rangle\right\}, \tag{14}$$

and e is the electron charge. The resulting (exact) equations of motion for the diagonal elements of $\sigma(t)$ are given by:

$$\frac{\partial}{\partial t}\sigma_{ii}\left(t\right)=-\frac{1}{\hbar^2}\sum_m\int_0^t d\tau\kappa_{ii,mm}\left(\tau\right)\sigma_{mm}\left(t-\tau\right). \tag{15}$$

If the coherences of $\sigma(t)$ are of interest, then one requires the off-diagonal elements of $\Phi_{ij,nm}(t)$, which are given by $\Phi_{ij,nm}(t)=\delta_{j1}\delta_{i0}\psi_{mn}(t)+\delta_{j0}\delta_{i1}\psi_{nm}^*(t)$, where

$$\begin{aligned}\psi_{mn}(t)=Tr_B\Big\{&\rho_B\langle n|\sum_k t_k a_k^\dagger(t)\\&-d^\dagger(t)\sum_\alpha M_\alpha\left(b_\alpha^\dagger(t)+b_\alpha(t)\right)|m\rangle\Big\}.\end{aligned} \tag{16}$$

In the above equations, the indices i, j, m, and n can take the values 1 or 0, corresponding to an occupied or an unoccupied dot, respectively.

IV. RESULTS

We first address the question of whether $\sigma(t)$ has a unique steady-state solution for different initial electronic preparation of the dot. In this case, if $\sigma(t)$ has a steady-state solution as $t \to \infty$, then

$$\frac{\partial}{\partial t}\sigma_{ii}(t) = 0 \tag{17}$$

and

$$\sum_m \int_0^\infty d\tau \kappa_{ii,mm}(\tau)\,\sigma_{mm}(t-\tau) = 0 \tag{18}$$

can be replaced by a linear set of equations given by:

$$\sum_m \mathcal{K}_{im}\sigma_m = 0, \tag{19}$$

where

$$\mathcal{K}_{im} = \frac{1}{\hbar^2}\int_0^\infty d\tau \kappa_{ii,mm}(\tau) \tag{20}$$

and $\sigma_m \equiv \sigma_{mm}(t \to \infty)$. The steady state is given by the eigenvector of matrix $\mathcal{K}$ with a zero eigenvalue. The analysis shows that this eigenvalue is nondegenerate and has an eigenvector given by $\sigma_{00} = \frac{\mathcal{K}_{00}}{\mathcal{K}_{00}+\mathcal{K}_{11}}$ and $\sigma_{11} = 1-\sigma_{00} = \frac{\mathcal{K}_{11}}{\mathcal{K}_{00}+\mathcal{K}_{11}}$. For a physical steady-state solution, both $\mathcal{K}_{00}$ and $\mathcal{K}_{11}$ must share the same sign. Otherwise, the diagonal elements of σ cannot both be positive. Since the steady-state depends only on the value of $\mathcal{K}_{00}$ and $\mathcal{K}_{11}$ and since both are independent of the initial dot population, the steady-state is independent of the initial preparation of the dot occupation and is therefore unique.

The above consideration shows that the steady-state is unique with respect to the electronic initial preparation. This is a strong statement by itself, but it does not rule out bistability for different initial phonon preparations. To address this question, we combined the formalism described above for the RDM with the ML-MCTDH approach in second quantized representation (SQR)[23,28]. The ML-MCTDH-SQR method provides a tool to compute the currents in Eq.(14) numerically exactly. The kernel $\kappa(t)$ is then obtained by numerically solving Eq. (12). In comparison, for most model parameters studied in this work, it is practically impossible to obtain converged values for the RDM directly from the ML-MCTDH-SQR, since the time to reach a steady-state solution is significantly longer than the maximum simulation time reachable by the ML-MCTDH-SQR. However, since the memory kernel decays on much shorter timescales compared to the RDM itself[24], it is rather straightforward to calculate it using the ML-MCTDH-SQR and then solve Eq. (15) for the RDM.

To characterize the population dynamics, we start with a factorized initial condition of the form

$$\rho(0) = \sigma(0) \otimes \rho_{\rm ph}(0) \otimes \rho_{\rm leads}(0), \tag{21}$$

where $\sigma(0)$ determines whether the electronic level is initially occupied/unoccupied,

$$\rho_{\rm ph}(0) = \exp\left[-\beta\left\{\sum_\alpha \omega_\alpha\left(b_\alpha^\dagger b_\alpha + \frac{1}{2}\right) + \sum_\alpha \delta_\alpha\left(b_\alpha^\dagger + b_\alpha\right)\right\}\right] \tag{22}$$

represents the initial density matrix of the phonon bath. Hereby two values of the parameters δ_α are considered: $\delta_\alpha = 0$ (corresponding to a phonon initial state equilibrated with an unoccupied dot) and $\delta_\alpha = \sqrt{2\omega_\alpha\lambda}$ (corresponding to phonons equilibrated to an occupied dot). The initial density matrix for the leads is given by:

$$\rho_{\rm leads}(0) = \exp\left[-\beta\left(\sum_{k\in L}(\varepsilon_k - \mu_L)\,a_k^\dagger a_k + \sum_{k\in R}(\varepsilon_k-\mu_R)\,a_k^\dagger a_k\right)\right]. \tag{23}$$

In the above equations $\beta = \frac{1}{k_B T}$ is the inverse temperature. In all results shown below we take $T = 0$ and apply a finite bias of $eV = \mu_L - \mu_R = 0.1\text{eV} = \frac{5}{8}\Gamma$, where Γ is the maximum value of $\Gamma_L + \Gamma_R$.

In Fig. 1 we plot the time evolution of $\sigma_{11}(t)$ (lower panels) and the corresponding nonzero elements of the memory kernel (upper panels), for two different initial vibrational preparations. We show the time evolution of $\sigma_{11}(t)$ for different values of the cutoff time t_c at which we assume that the memory kernel has essentially decayed to zero, such that it can be safely truncated. For $\delta_\alpha = 0$, it is safe to truncate the memory kernel at $t_c > 30\text{fs} = 7.5/\Gamma$ while $\delta_\alpha = \sqrt{2\omega_\alpha\lambda}$ requires a larger cutoff time of $t_c > 80\text{fs} = 20/\Gamma$. In both case, the cutoff time is much larger than $\frac{1}{\mu_L-\mu_R}$. Comparing the time it takes for the memory kernel to decay (upper panels of Fig. 1) with the time taken by the RDM to reach steady-state (corresponding lower panels of Fig. 1), it is clear that the latter is slower by nearly an order of magnitude and in some cases even more. Since the calculation of the memory kernel using the ML-MCTDH-SQR method is by far the most time consuming portion of the calculation, the combination with the RDM formalism provides a significant saving, and more importantly extends the ML-MCTDH-SQR approach to regimes inaccessible by direct application.

The inset of Fig. 1 shows the steady-state value of σ_{11} as a function of $1/t_c$ for $\delta_\alpha = \sqrt{2\omega_\alpha\lambda}$. For large values of $1/t_c$ (short cutoff times) we find that the formalism may lead to unphysical situations in which σ_{11} becomes negative. Of course, this is expected, since only when the memory kernel has decayed to zero does the cutoff approximation provide a physically meaningful solution. As $1/t_c$ decreases σ_{11} converges and approaches a plateau value. In the present case of parameters, the steady-state value of σ_{11} computed for the two initial vibrational states roughly coincides. However, the dynamics and timescales to relax to the steady-state are clearly sensitive to the initial vibrational preparation.

In Fig. 2 we plot $\sigma_{11}(t)$ for four different values of characteristic phonon frequency ω_c and compare the time de-

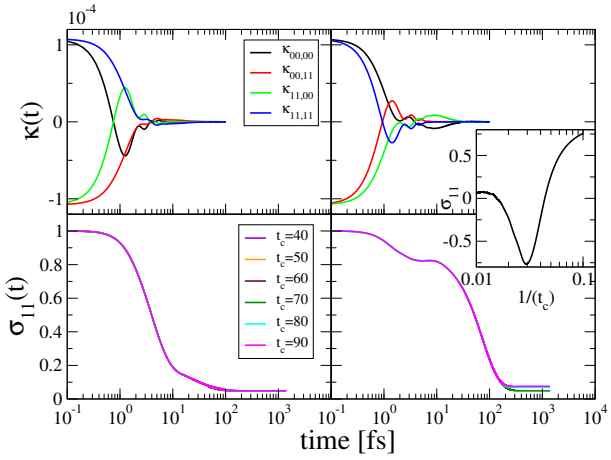

Figure 1: The occupation of the quantum dot $\sigma_{11}(t)$ (lower panels) for different cutoff times and the nonzero elements of the memory kernel (upper panels) for $\delta_\alpha = 0$ (left panels) and $\delta_\alpha = \sqrt{2\omega_\alpha\lambda}$ (right panels). The inset shows the steady-state value of σ_{11} for the case of $\delta_\alpha = \sqrt{2\omega_\alpha\lambda}$ as a function of $1/t_c$. The model parameters used are: $\varepsilon_d = 0.5$eV, $\omega_c = 500\text{cm}^{-1}$, and $\lambda = 3000\text{cm}^{-1}$.

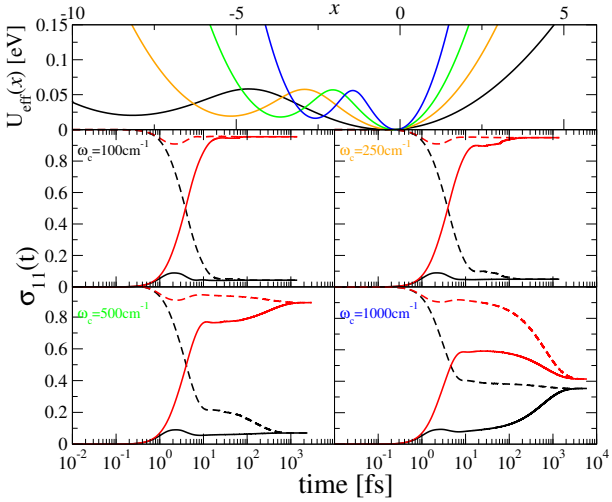

Figure 2: Plots of the occupation of the quantum dot $\sigma_{11}(t)$ for different ω_c. The solid black, dashed black, solid red, and dashed red curves correspond to $\{n_d = 0, \delta_\alpha = 0\}$, $\{n_d = 1, \delta_\alpha = 0\}$, $\{n_d = 0, \delta_\alpha = \sqrt{2\omega_\alpha\lambda}\}$, and $\{n_d = 1, \delta_\alpha = \sqrt{2\omega_\alpha\lambda}\}$, respectively. Upper panel shows the adiabatic effective potentials for the different values of ω_c. The model parameters used are: $\varepsilon_d = 0.5$eV, and $\lambda = 4000\text{cm}^{-1}$.

pendence for four different initial conditions, corresponding to an initial empty ($n_d = 0$) or occupied ($n_d = 1$) dot and to $\delta_\alpha = 0$ or $\delta_\alpha = \sqrt{2\omega_\alpha\lambda}$. For a given δ_α (i.e. a fixed initial state for the phonons), we find that $\sigma_{11}(t)$ has a unique steady-state solution regardless of the initial dot occupation. This numerically converged result is consistent with the analytical proof given above. In contrast, for two different initial states of the phonons, a clear bistability is observed even at a finite bias, and the RDM decays to a different steady-state solution depending on the value of δ_α.

The appearance of a bistability is consistent with predictions based on a mean field treatment, which is accurate in the adiabatic limit where $\omega_c \to 0$[5]. For all four frequencies studied, the adiabatic effective potentials[29] shows two distinct minima (upper panel of Fig. 2), corresponding to two possible stable configurations[30]. The height of the barrier between the two minima is independent of the phonon frequency, however, as clearly evident in the figure, the width of the barrier increases as ω_c decreases. This implies that the tunneling time between the two configurations also increases as ω_c decreases. As a results, the extent of bistability (given by the difference between σ_{11} at steady-state for $\delta_\alpha = 0$ and $\delta_\alpha \neq 0$) increases with decreasing ω_c, as shown in Fig. 2. The transient dynamics and the approach to steady state depends sensitively on the preparation, in particular, whether the initial state is close to equilibrium ($\{n_d = 0, \delta_\alpha = 0\}$ and $\{n_d = 1, \delta = \sqrt{2\omega_\alpha\lambda}\}$) or far from equilibrium ($\{n_d = 0, \delta_\alpha = \sqrt{2\omega_\alpha\lambda}\}$ and $\{n_d = 1, \delta_\alpha = 0\}$). For small ω_c we observe a rapid decay to steady state on a time scale $\hbar\Gamma^{-1}$, where Γ denotes the maximum of leads spectral function. As ω_c increases, the dynamics become more complex. In particular, a longer time scale in the relaxation of $\sigma_{11}(t)$ develops, consistent with the appearance of a slow tunneling channel between the two configurations as discussed above. However, over the time scale considered, the existence of this channel does not lead to a unique steady state solution for the populations at a finite value of ω_c, even away from the adiabatic limit.

We next consider in Fig. 3 the influence of the electron-phonon coupling strength λ and the dot energy ε_d on the nonequilibrium dynamics. As before, we compare the time dependence of $\sigma_{11}(t)$ for four different initial conditions. In the upper panel we show the corresponding adiabatic effective potentials[29] for the four values of λ. For small values of λ, the bistability clearly disappears (left panels of Fig 3). This is consistent with the fact that the adiabatic effective potential has a single minimum for $\lambda \leq 3000\text{cm}^{-1}$ (in fact, a crude estimate based on a mean-field approach suggests that below $\lambda = 3150\text{cm}^{-1}$ the bistability vanishes for the current parameters). Comparing the relaxation time for $\lambda = 2000\text{cm}^{-1}$ and $\lambda = 3000\text{cm}^{-1}$, we find that the latter is slower, particularly for the case of $\delta_\alpha = \sqrt{2\omega_\alpha\lambda}$.

When λ is further increased to 4000cm^{-1} (corresponding to a nearly symmetric case where the polaron shift equals ε_d) the relaxation time stretches even more and the system decays to a different steady-state depending on the value of δ_α, again consistent with the appearance of two stable configurations in the corresponding adiabatic effective potential (upper panel of Fig. 3). While the RDM shows a distinct bistability, it is interesting to note that this is not the case for the current through the quantum dot (not shown), which for the symmetric case ($\lambda \approx \varepsilon_d$) has the same value for the two different states

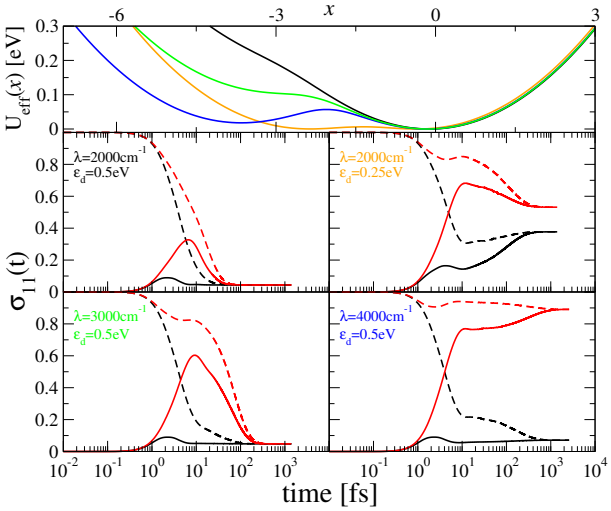

Figure 3: Similar to Fig. 2 but for different values of λ and ε_d, for $\omega_c = 500\text{cm}^{-1}$. Upper panel shows the adiabatic effective potentials for the different values of λ.

of the RDM.

In the upper right panel of Fig. 3 we show results for the case where $\lambda = 2000\text{cm}^{-1}$ and $\varepsilon_d = 0.25\text{eV}$. The effective adiabatic potential for this case clearly shows two distinct minima, however, the barrier is lower than $\lambda = 4000\text{cm}^{-1}$ and $\varepsilon_d = 0.5\text{eV}$. Comparing the two right panels of Fig. 3, we find that as λ and ε_d are decreased simultaneously, the bistability decreases and the timescale to relax to steady-state also decreases, consistent with the adiabatic tunneling picture discussed above.

The time-dependent approach developed here describes the nonequilibrium dynamics numerically exactly only over a certain time scale (related to the cutoff time). Perhaps on timescales much larger than that accessible by the current approach (i.e., larger than $500/\Gamma$), long-ranged memory effects not captured by the cutoff approximation may result in switching between the different states and lead to a unique steady state. This is certainly expected for strong nonequilibrium situations (large voltage) and/or high temperature and preliminary results indicate that at higher bias voltages the bistability vanishes. Whether this is also the case for zero temperature and smaller bias voltages, as predicted by approximate methods for a single phonon[4,31], is an open question. In this respect, we find that the bistability persists even for a finite bias assuming that beyond the cutoff time the memory kernel decays as a power law (t^{-2}).

V. SUMMARY

We have studied nonequilibrium dynamics of a many-body quantum system with electron-phonon interactions employing a numerically exact method based on combination of a RDM formalism with the ML-MCTDH-SQR method. For a generic model, which is widely used to describe phonon-coupled electron transport in quantum dots and single-molecule junctions, we showed that the system may exhibit pronounced bistability even in *out-of-equilibrium* situations, when the value of the bias is far from the linear response regime ($eV \approx \Gamma$). The analysis reveals that the bistability increases for decreasing phonon frequency and depends sensitively on the electron-phonon coupling. Based on the RDM formalism, we proved that the bistability is associated with different initial phonon preparations and not with a different initial dot occupation. In all cases the bistability develops on time scales much longer than the typical bare energy scales, in particular $(\mu_L - \mu_R)\tau >> 1$ and $\Gamma\tau >> 1$, where τ is the observed relaxation time. Furthermore, we find that the phenomenon persists over time scales of $\approx 500/\Gamma$, which are much longer than the typical phonon time scales and in some cases also longer than the phonon tunneling time. Therefore, the phenomenon should also be accessible experimentally with ultrafast spectroscopy techniques.

Acknowledgments

We would like to thank Michael Galperin, Abe Nitzan, David Reichman, and Avi Schiller for useful discussion. EYW is grateful to The Center for Nanoscience and Nanotechnology at Tel Aviv University for a doctoral fellowship. HW acknowledges the support from the National Science Foundation CHE-1012479. GC is grateful Yad Hanadiv Rothschild Foundation for the award of a Rothschild Fellowship. MT and ER are grateful to the Institute of Advanced Studies at the Hebrew University for the warm hospitality. This work was supported by the FP7 Marie Curie IOF project HJSC, by the DFG (SFB 953 and cluster of excellence EAM), and used resources of the National Energy Research Scientific Computing Center, which is supported by the Office of Science of the U.S. Department of Energy under Contract No. DE-AC02-05CH11231.

[1] B. Doyon and N. Andrei, Phys. Rev. B **73**, 245326 (2006).
[2] S. Kurth, G. Stefanucci, E. Khosravi, C. Verdozzi, and E. K. U. Gross, Phys. Rev. Lett. **104**, 236801 (2010).
[3] M. Galperin, M. A. Ratner, and A. Nitzan, Nano Lett. **5**, 125 (2004).
[4] A. Mitra, I. Aleiner, and A. Millis, Phys. Rev. Lett. **94**, 076404 (2005).
[5] M. Galperin, A. Nitzan, and M. A. Ratner, J. of Phys.: Condens. Matter **20**, 374107 (2008).
[6] A. S. Alexandrov and A. M. Bratkovsky, J. Phys. Condens. Matter **19**, 255203 (2007).
[7] A. S. Alexandrov and A. M. Bratkovsky, Phys. Rev. B **80**,

115321 (2009).
[8] A. A. Dzhioev and D. S. Kosov, J. Chem. Phys. **135**, 174111 (2011).
[9] K. F. Albrecht, H. Wang, L. Mühlbacher, M. Thoss, and A. Komnik, Phys. Rev. B **86**, 081412 (2012).
[10] A. O. Gogolin and A. Komnik, "Multistable transport regimes and conformational changes in molecular quantum dots," *arXiv* 0207513.
[11] K. F. Albrecht, A. Martin-Rodero, R. C. Monreal, L. Mühlbacher, and A. Levy Yeyati, Phys. Rev. B **87**, 085127 (2013).
[12] F. B. Anders and A. Schiller, Phys. Rev. Lett. **95**, 196801 (2005).
[13] P. Schmitteckert, Phys. Rev. B **70**, 121302 (2004).
[14] S. R. White, Phys. Rev. Lett. **69**, 2863 (1992).
[15] F. A. Andre Jovchev, arXiv:cond-mat/1302.0184(2013).
[16] S. Weiss, J. Eckel, M. Thorwart, and R. Egger, Phys. Rev. B **77**, 195316 (2008).
[17] J. Eckel, F. Heidrich-Meisner, S. G. Jakobs, M. Thorwart, M. Pletyukhov, and R. Egger, New J. Phys. **12**, 043042 (2010).
[18] D. Segal, A. J. Millis, and D. R. Reichman, Phys. Rev. B **82**, 205323 (2010).
[19] L. Mühlbacher and E. Rabani, Phys. Rev. Lett. **100**, 176403 (2008).
[20] P. Werner, T. Oka, and A. J. Millis, Phys. Rev. B **79**, 035320 (2009).
[21] M. Schiró and M. Fabrizio, Phys. Rev. B **79**, 153302 (2009).
[22] P. Werner, T. Oka, M. Eckstein, and A. J. Millis, Phys. Rev. B **81**, 035108 (2010).
[23] H. Wang, I. Pshenichnyuk, R. Härtle, and M. Thoss, J. Chem. Phys. **135**, 244506 (2011).
[24] G. Cohen and E. Rabani, Phys. Rev. B **84**, 075150 (2011).
[25] H. Wang and M. Thoss, J. Chem. Phys. **119**, 1289 (2003).
[26] J. C. Cuevas and E. Scheer, *Molecular Electronics: An Introduction to Theory and Experiment* (World Scientific, Singapore, 2010).
[27] M.-L. Zhang, B. J. Ka, and E. Geva, The Journal of Chemical Physics **125**, 044106 (2006).
[28] H. Wang and M. Thoss, J. Chem. Phys. **131**, 024114 (2009).
[29] A. A. Dzhioev and D. S. Kosov, J. Chem. Phys. **135**, 074701 (2011).
[30] To obtain the adiabatic potential the multiphonon problem was represented by a single mode with potential $U(x) = \frac{1}{2}\omega_c x^2$. The adiabatic effective potential is then given by the integral over the mean force $U_{\text{eff}}(x) = U(x) + \int dx \varepsilon'(x) n(x)$ where $\varepsilon(x) = \varepsilon_d + M_c x$ is the dot energy at position x, and $n(x) = -\frac{i\hbar}{2\pi}\int_{\infty}^{\infty} d\omega G^{<}(\omega, x)$, where $G^{<}(\omega, x)$ is the lesser Green function for a fixed phonon coordinate obtained by solving the nonequilibrium Green function on the Keldysh contour (see Ref. [26]).
[31] F. Pistolesi, Y. M. Blanter, and I. Martin, Phys. Rev. B **78**, 085127 (2008).